

# Energy Beamforming for RF Wireless Power Transfer with Dynamic Metasurface Antennas

Amirhossein Azarbahram, *Student Member, IEEE*, Onel L. A. López, *Member, IEEE*

Richard D. Souza, *Senior Member, IEEE*, Rui Zhang, *Fellow, IEEE*, and Matti Latva-Aho, *Senior Member, IEEE*

**Abstract**—Radio frequency (RF) wireless power transfer (WPT) is a promising technology for Internet of Things networks. However, RF-WPT is still energy inefficient, calling for advances in waveform optimization, distributed antenna, and energy beamforming (EB). In particular, EB can compensate for the severe propagation loss by directing beams toward the devices. The EB flexibility depends on the transmitter architecture, existing a trade-off between cost/complexity and degrees of freedom. Thus, simpler architectures such as dynamic metasurface antennas (DMAs) are gaining attention. Herein, we consider an RF-WPT system with a transmit DMA for meeting the EH requirements of multiple devices and formulate an optimization problem for the minimum-power design. First, we provide a mathematical model to capture the frequency-dependant signal propagation effect in the DMA architecture. Next, we propose a solution based on semi-definite programming and alternating optimization. Results show that a DMA-based implementation can outperform a fully-digital structure and that utilizing a larger antenna array can reduce the required transmit power, while the operation frequency does not influence much the performance.

**Index Terms**—Radio frequency wireless power transfer, dynamic metasurface antennas, energy beamforming.

## I. INTRODUCTION

**F**UTURE wireless systems must support the uninterrupted operation of massive Internet of Things networks. This requires a reliable energy supply for low-power wireless devices. Radio frequency (RF) wireless power transfer (WPT) technology is a promising solution to achieve this goal, as it allows charging multiple energy harvesting (EH) devices using the same infrastructure, similar to simultaneously transmitting multiple data streams in wireless communication [1]–[3].

The end-to-end power transfer efficiency of an RF-WPT system is inherently low, calling for efficient techniques such as waveform optimization, energy beamforming (EB), and distributed antenna systems [3], [4]. Notably, EB can compensate for propagation loss by focusing energy beams toward one or

more EH devices at the same time. The EB flexibility and potential gains are determined by the transmitter architecture. Although a fully digital (FD) structure provides the highest flexibility, it requires a large number of RF chains, resulting in high complexity and cost. The analog architecture alternatives incur much lower power consumption and cost as they utilize only analog circuits, as phase shifters. However, they may not offer sufficient flexibility. Thus, hybrid architectures have been introduced to combine digital and analog approaches and provide beamforming capability with a reasonable trade-off between complexity/cost and flexibility [5], [6].

In hybrid architectures, the complexity and losses of analog circuits affect scalability and performance. To address this issue, an array of subarrays (AoSA) is used in [7] to reduce the analog part complexity. A dynamic AoSA is proposed in [8] to improve energy efficiency. Other new technologies have been proposed to avoid analog circuits, such as the dynamic metasurface antenna (DMA), which consists of a group of configurable metamaterial elements placed on a set of waveguides [9]. DMA is utilized in [10] in near-field WPT to maximize the sum-harvested energy considering linear RF-to-DC conversion. However, in practice, there are extensive nonlinearities in the EH device. A practical alternative is to meet an RF power requirement for each device so that it applies to any nonlinear EH relationship simply by obtaining the RF power from the DC requirement.

In this letter, we consider a DMA transmitter architecture to charge multiple single-antenna EH devices. Our main contributions are as follows: i) we formulate the EB optimization problem aiming to minimize the transmit power while meeting the EH requirements of all energy receivers; ii) we provide a frequency dependant model for the propagation characteristics of the DMA, which was overlooked in the previous studies; iii) we propose an efficient EB solution relying on semi-definite programming (SDP) and alternating optimization, which converges in polynomial time; iv) we show that DMA outperforms the FD structure in terms of minimum transmit power for meeting the EH requirements, and increasing the antenna array size can reduce the transmit power, while the operating frequency does not affect much the system performance.

**Notations:** Bold lowercase and upper-case letters represent vectors and matrices, respectively. The notation  $|\cdot|$  denotes the  $l_2$  norm of a vector, while  $(\cdot)^T$  and  $(\cdot)^H$  indicate the transpose and transpose conjugate of a matrix or vector, respectively. The mathematical expectation is represented by  $\mathbb{E}$ , and  $\otimes$  refers to the Kronecker product. Moreover,  $\text{rank}(\cdot)$  and  $\text{Tr}(\cdot)$  are the rank and trace of a matrix, respectively. Finally, the

A. Azarbahram, O. López and M. Latva-Aho, Centre for Wireless Communications (CWC), University of Oulu, Finland, {amirhossein.azarbahram, onel.alcarazlopez, matti.latva-aho}@oulu.fi; R. D. Souza, Department of Electrical and Electronics Engineering, Federal University of Santa Catarina, Florianopolis, Brazil, richard.demo@ufsc.br; R. Zhang, School of Science and Engineering, Shenzhen Research Institute of Big Data, The Chinese University of Hong Kong, Shenzhen, Guangdong, China, rzhang@cuhk.edu.cn, and Department of Electrical and Computer Engineering, National University of Singapore, Singapore, elezhang@nus.edu.sg.

This work is partially supported in Finland by the Finnish Foundation for Technology Promotion, Academy of Finland (Grants 348515 and 346208 (6G Flagship)), by the European Commission through the Horizon Europe/JU SNS project Hexa-X-II (Grant Agreement no. 101095759); and in Brazil by CNPq (402378/2021-0, 401730/2022-0, 305021/2021-4) and RNP/MCTIC 6G Mobile Communications Systems (01245.010604/2020-14).

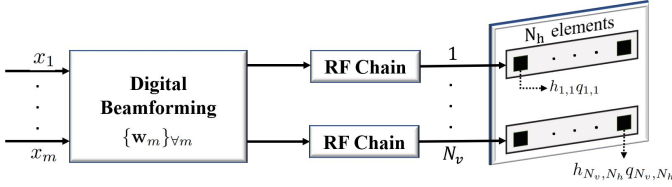


Fig. 1: DMA-based transmitter architecture.

vectorization operation is written as  $\text{Vec}(\cdot)$ .

## II. SYSTEM MODEL & PROBLEM FORMULATION

We consider a multi-antenna RF-WPT system where a transmitter equipped with a DMA uniform square array charges  $K$  single-antenna devices. As illustrated in Fig. 1,  $M$  energy symbols are the inputs of a digital beamformer, while there are  $N_v$  RF chains at the output. Each RF chain is connected to a waveguide consisting of  $N_h$  metamaterial elements positioned on it; thus, the total number of metamaterial elements is  $N = N_v \times N_h$ .

We consider the near-field wireless channel. The  $k$ -th user, located at a distance  $r_k$  from the transmitter, lies in the near-field propagation region if  $d_{fs} < r_k < d_{fr}$ , where  $d_{fs} = \sqrt[3]{\frac{D^4}{8\lambda}}$  and  $d_{fr} = \frac{2D^2}{\lambda}$  are the Fresnel and Fraunhofer distance, respectively. Moreover,  $\lambda$  is the wavelength,  $D = \sqrt{2}L$  is the antenna diameter, and  $L$  is the antenna length. The location of the  $l$ th element in the  $i$ th waveguide is  $\mathbf{p}_{i,l} = [x_{i,l}, y_{i,l}, z_{i,l}]^T$ ,  $i = 1, 2, \dots, N_v$  and  $l = 1, 2, \dots, N_h$ . Additionally,  $\mathbf{p}_k$  denotes the  $k$ th user location.

The channel coefficient between user  $k$  and the  $l$ th metamaterial element in the  $i$ th waveguide is given by [11]

$$\gamma_{i,l,k} = A_{i,l,k} e^{-\frac{j2\pi}{\lambda} d_{i,l,k}}, \quad (1)$$

where  $2\pi d_{i,l,k}/\lambda$  constitutes the phase shift introduced by the propagation distance, and  $d_{i,l,k} = |\mathbf{p}_k - \mathbf{p}_{i,l}|$  is the Euclidean distance between the element and the user. Additionally, the channel gain coefficient is

$$A_{i,l,k} = \sqrt{F(\theta_{i,l,k}, \phi_{i,l,k})} \frac{\lambda}{4\pi d_{i,l,k}}, \quad (2)$$

where  $\theta_{i,l,k}$  and  $\phi_{i,l,k}$  are the elevation and azimuth angle, respectively, while  $F(\theta_{i,l,k}, \phi_{i,l,k})$  denotes the radiation profile of each element. We assume that the latter is given by [12]

$$F(\theta_{i,l,k}, \phi_{i,l,k}) = \begin{cases} G_t \cos(\theta_{i,l,k})^{\frac{G_t}{2}-1}, & \theta_{i,l,k} \in [0, \frac{\pi}{2}], \\ 0, & \text{otherwise,} \end{cases} \quad (3)$$

where  $G_t = 2(b+1)$  and  $b$  are the transmit antenna gain and the boresight gain, respectively. Now, let us define  $\boldsymbol{\gamma}_k = [\gamma_{1,1,k}, \gamma_{1,2,k}, \dots, \gamma_{N_v, N_h, k}]^T$  as the  $N$ -dimensional channel coefficients vector between the user  $k$  and the elements of the DMA. Note that under the conventional far-field conditions, the channel coefficient can be represented as  $A_k e^{-j\psi_{i,l,k}}$ , where  $A_k$  is only determined by the distance between the user and the antenna array, and  $\psi_{i,l,k}$  by the spatial direction of the user and the spacing between the antenna elements.

Table I: Microstrip material characteristics.

Material	$\epsilon_r$	$\varrho$	Typical $\zeta$
©Cylex FR4 @50Hz	5.5	0.04	1.6 mm
©DuPont Pyralux AP-9161 @1MHz	3.4	0.002	0.15 mm
©Rogers RO4003C @2.5GHz	3.55	0.0021	0.53 mm
©Taconic RF-10 @10GHz	10.2	0.0025	0.25 mm
©Sytech LNB33C @10GHz	3.5	0.0035	0.78 mm
©Ventec VT-870 H348 TCR @10GHz	3.48	0.0037	0.17 mm
©Panasonic R-5515 @14, 26GHz	3	0.002	0.105 mm
©Panasonic R-5515 @37, 48, 60GHz	3	0.003	0.105 mm
©Isola IS580G @5, 10, 20GHz	3.8	0.006	0.4 mm
©Arlon AD260A @1 MHz	2.6	0.00135	1.14 mm
©Arlon AD260A @10 GHz	2.6	0.0017	1.14 mm

### A. DMA Model

In practice, microstrip lines are usually utilized as the DMA waveguides. The propagation coefficient for the  $l$ th element in the  $i$ th microstrip is given by [13]

$$h_{i,l} = e^{-(l-1)d_l(\alpha_i + j\beta_i)}, \quad (4)$$

where  $d_l$ ,  $\alpha_i$ , and  $\beta_i$  are the inter-element distance, waveguide attenuation coefficient, and propagation constant, respectively. We assume that all microstrips are of the same type;  $\beta_i = \beta$  and  $\alpha_i = \alpha$ . In general, the frequency of the system affects the signal propagation inside a waveguide, and hence, the propagation model must capture the frequency-dependent effects.

The microstrip line comprises a conductor of width  $v$ , printed on a dielectric substrate with thickness  $\zeta$  and dielectric constant  $\epsilon_r$ . Thus, the effective dielectric constant at DC is [14]

$$\epsilon'_e = \frac{\epsilon_r + 1}{2} + \frac{\epsilon_r - 1}{2} \frac{1}{\sqrt{1 + 12\frac{\zeta}{v}}}. \quad (5)$$

The effective dielectric constant at frequency  $f$  is [14]

$$\epsilon_e^f = \epsilon_r - \frac{\epsilon_r - \epsilon'_e}{1 + G(f)}, \quad (6)$$

where  $G(f) = \frac{(0.6 + 0.009Z_0)f^2}{(Z_0/8\pi\zeta)^2}$ , and

$$Z_0 = \begin{cases} \frac{60}{\sqrt{\epsilon_e^f}} \ln\left(\frac{8\zeta}{v} + \frac{v}{4\zeta}\right), & \frac{v}{\zeta} \leq 1, \\ \frac{120\pi}{\sqrt{\epsilon_e^f} \left[\frac{v}{\zeta} + 1.393 + 0.667 \ln\left(\frac{v}{\zeta} + 1.444\right)\right]}, & \frac{v}{\zeta} \geq 1, \end{cases} \quad (7)$$

is the characteristic impedance of the microstrip. Thereby,  $\beta = \frac{2\pi}{\lambda} \sqrt{\epsilon_e^f}$  is the microstrip propagation constant and the attenuation due to the dielectric loss is given by

$$\alpha_d = \frac{k_0 \epsilon_r (\epsilon_e^f - 1) \varrho}{2\sqrt{\epsilon_e^f} (\epsilon_r - 1)}, \quad (8)$$

where  $\varrho$  is the loss tangent of the dielectric. Moreover,  $\alpha_c = R_s/Z_0 v$  is the approximate attenuation due to the conductor loss and  $R_s = \sqrt{2\pi f \mu_0 / 2\sigma}$  is the conductor surface resistivity with  $\sigma$  and  $\mu_0$  being the conductivity and the free space permeability, respectively. Finally, the microstrip line attenuation coefficient is modeled as  $\alpha = \alpha_d + \alpha_c$ . Table I lists some microstrip materials with their main parameters and the frequencies at which they were computed<sup>1</sup>.

<sup>1</sup>The typical  $\zeta$  serves as an indicator of the product thickness range.

Next,  $\mathbf{H} \in \mathbb{C}^{N \times N}$  is the microstrip propagation diagonal matrix with  $h_{i,l}$  being the  $((i-1)N_h + l)$ th column and  $((i-1)N_h + l)$ th row element. The Lorentzian-constrained phase model is utilized to capture the dependency between the elements amplitude and phase [13], so that the frequency response of the  $l$ th element in the  $i$ th microstrip is

$$q_{i,l} \in \mathcal{Q} = \left\{ \frac{j + e^{j\phi_{i,l}}}{2} \mid \phi_{i,l} \in [0, 2\pi] \right\}, \quad \forall i, l. \quad (9)$$

Additionally,  $\mathbf{Q} \in \mathbb{C}^{N \times N_d}$  is the matrix containing the configurable weights of the metamaterial elements [11], i.e.,

$$\mathbf{Q}_{(i-1)N_h+l,n} = \begin{cases} q_{i,l}, & i = n, \\ 0, & i \neq n. \end{cases} \quad (10)$$

### B. Signal Model

Let  $x_m$  be the  $m$ th energy symbol at the input of the digital precoder where  $m = 1, \dots, M$  and  $M = \min(N_v, K)$ . Also, the energy symbols are independent and normalized such that  $\mathbb{E}\{x_n^H x_r\} = 0$  and  $\mathbb{E}\{x_n^H x_n\} = 1$ , while  $\mathbf{w}_m$  is the  $N_v$ -dimensional precoding vector for  $x_m$ . Thus, the transmit signal is  $\mathbf{s} = \sum_{m=1}^M \mathbf{H}\mathbf{Q}\mathbf{w}_m x_m$ , while the transmit power is

$$P_{Tx} = \mathbb{E}_x \{ \mathbf{s}^H \mathbf{s} \} = \sum_{m=1}^M |\mathbf{H}\mathbf{Q}\mathbf{w}_m|^2. \quad (11)$$

The received energy signal at the  $k$ th EH device is given by  $y_k = \gamma_k^H \mathbf{s}$ , while the corresponding received RF power is

$$P_{Rx}^k = \mathbb{E}_x \{ y_k^H y_k \} = \sum_{m=1}^M |\gamma_k^H \mathbf{H}\mathbf{Q}\mathbf{w}_m|^2. \quad (12)$$

### C. Problem Formulation

The EB design objective is to minimize the transmit power while satisfying the user's EH requirements. Assuming the location of the users is known, the optimization problem is

$$\mathbf{P1} : \quad \underset{\mathbf{Q}, \{\mathbf{w}_m\}, \forall m}{\text{minimize}} \quad \sum_{m=1}^M |\mathbf{H}\mathbf{Q}\mathbf{w}_m|^2 \quad (13a)$$

$$\text{subject to} \quad \sum_{m=1}^M |\gamma_k^H \mathbf{H}\mathbf{Q}\mathbf{w}_m|^2 \geq \delta_k, \quad \forall k, \quad (13b)$$

$$(10), \quad q_{i,l} \in \mathcal{Q}, \quad \forall i, l. \quad (13c)$$

where  $\delta_k$  is the RF power required by  $k$ th user, which can be obtained from the DC harvesting requirement using any practical EH model. Notice that the problem constraints are non-convex and the optimization variables are highly coupled, due to the correlation between the phase and amplitude of the metamaterial elements through the Lorentzian constraint, thus making (13) very difficult to be optimally solved.

## III. PROPOSED EB OPTIMIZATION SOLUTION

Next, we utilize alternating optimization to cope with the complexity of problem (13).

### A. Optimal Digital Precoders with Fixed $\mathbf{Q}$

Let us fix  $\mathbf{Q}$  and rewrite (12) as

$$\begin{aligned} P_{Rx}^k &= \sum_{m=1}^M (\mathbf{w}_m^T (\gamma_k^H \mathbf{H}\mathbf{Q})^T)^H (\mathbf{w}_m^T (\gamma_k^H \mathbf{H}\mathbf{Q})^T) \\ &= ((\gamma_k^H \mathbf{H}\mathbf{Q})^H)^T \left[ \sum_{m=1}^M (\mathbf{w}_m^T)^H \mathbf{w}_m^T \right] (\gamma_k^H \mathbf{H}\mathbf{Q})^T \\ &= \mathbf{b}_k^T \left[ \sum_{m=1}^M \mathbf{w}_m^* \mathbf{w}_m^T \right] \mathbf{b}_k^* = \text{Tr}(\mathbf{W}^T \mathbf{B}_k), \end{aligned} \quad (14)$$

which comes from several algebraic transformations and by defining  $\mathbf{b}_k = (\gamma_k^H \mathbf{H}\mathbf{Q})^H \in \mathbb{C}^{N_d \times 1}$ ,  $\mathbf{W} = \sum_{m=1}^M \mathbf{w}_m \mathbf{w}_m^H$ , and  $\mathbf{B}_k = (\mathbf{b}_k \mathbf{b}_k^H)^T$ . Similarly, we reformulate (11) as

$$P_{Tx} = \text{Tr}(\mathbf{W}^T \mathbf{F}), \quad (15)$$

where  $\mathbf{F} = (\mathbf{H}\mathbf{Q})^H \mathbf{H}\mathbf{Q}$ . Therefore, by leveraging (14) and (15), (13) can be reformulated with a fixed  $\mathbf{Q}$  as

$$\mathbf{P2} : \quad \underset{\mathbf{W}}{\text{minimize}} \quad \text{Tr}(\mathbf{W}^T \mathbf{F}) \quad (16a)$$

$$\text{subject to} \quad \text{Tr}(\mathbf{W}^T \mathbf{B}_k) \geq \delta_k, \quad \forall k, \quad (16b)$$

$$\mathbf{W} \succeq \mathbf{0}, \quad (16c)$$

which is an SDP that can be solved by standard convex optimization tools, e.g., CVX [15]. Then, the optimal precoding vectors  $\{\mathbf{w}_m\}_{\forall m}$  can be obtained as the eigenvectors of  $\mathbf{W}$  multiplied by the square root of their respective eigenvalues.

### B. Suboptimal $\mathbf{Q}$ with Fixed Digital Precoders

Now, let us fix  $\{\mathbf{w}_m\}_{\forall m}$ . Then, utilizing the fact that  $\mathbf{a}^T \mathbf{G} \mathbf{b} = (\mathbf{b}^T \otimes \mathbf{a}^T) \text{Vec}(\mathbf{G})$ , we obtain [11]

$$|\gamma_k^H \mathbf{H}\mathbf{Q}\mathbf{w}_m|^2 = |(\mathbf{w}_m^T \otimes (\gamma_k^H \mathbf{H})) \mathbf{q}|^2 = |\mathbf{z}_{m,k}^H \mathbf{q}|^2, \quad (17)$$

$$|\mathbf{H}\mathbf{Q}\mathbf{w}_m|^2 = |(\mathbf{w}_m^T \otimes \mathbf{H}) \mathbf{q}|^2 = |\mathbf{P}_m^H \mathbf{q}|^2, \quad (18)$$

where  $\mathbf{q} = \text{Vec}(\mathbf{Q}) \in \mathbb{C}^{N N_v \times 1}$ ,  $\mathbf{P}_m = (\mathbf{w}_m^T \otimes \mathbf{H})^H \in \mathbb{C}^{N N_v \times N}$ , and  $\mathbf{z}_{m,k} = (\mathbf{w}_m^T \otimes (\gamma_k^H \mathbf{H}))^H \in \mathbb{C}^{N N_v \times 1}$ . Moreover, we define  $\hat{\mathbf{q}} \in \mathbb{C}^{N \times 1}$  as the modified version of  $\mathbf{q}$  without the zero elements, thus,  $\hat{\mathbf{q}} = [q_{1,1}, q_{1,2}, \dots, q_{N_v, N_h}]^T$ . Additionally,  $\hat{\mathbf{z}}_{m,k} \in \mathbb{C}^{N \times 1}$  is obtained by removing the elements with the same index as the zero elements in  $\mathbf{q}$ , while  $\hat{\mathbf{P}}_m \in \mathbb{C}^{N \times N}$  comes from removing the columns of  $\mathbf{P}_m$  with such indices. Then, the  $k$ th user received power is written as

$$\begin{aligned} P_{Rx}^k &\stackrel{(a)}{=} \sum_{m=1}^M (\mathbf{z}_{m,k}^H \mathbf{q})^H (\mathbf{z}_{m,k} \mathbf{q}) \\ &\stackrel{(b)}{=} \hat{\mathbf{q}}^H \left[ \sum_{m=1}^M \hat{\mathbf{z}}_{m,k}^H \hat{\mathbf{z}}_{m,k} \right] \hat{\mathbf{q}} \stackrel{(c)}{=} \text{Tr}(\tilde{\mathbf{Z}}_{m,k}^H \tilde{\mathbf{Q}}), \end{aligned} \quad (19)$$

where (a) comes from using (17) followed by a simple transformation and (b) from zeroing the terms impacted by the zero elements of  $\mathbf{q}$ . Furthermore, (c) comes from defining  $\tilde{\mathbf{Q}} = \hat{\mathbf{q}} \hat{\mathbf{q}}^H$  and  $\tilde{\mathbf{Z}}_{m,k} = \sum_{m=1}^M \hat{\mathbf{z}}_{m,k} \hat{\mathbf{z}}_{m,k}^H$ . Similarly, the transmit power can be written as  $P_{Tx} = \text{Tr}(\tilde{\mathbf{P}}_m^H \tilde{\mathbf{Q}})$ , where  $\tilde{\mathbf{P}}_m = \sum_{m=1}^M \hat{\mathbf{P}}_m \hat{\mathbf{P}}_m^H$ . Thereby, the optimization problem with fixed precoders can be formulated as

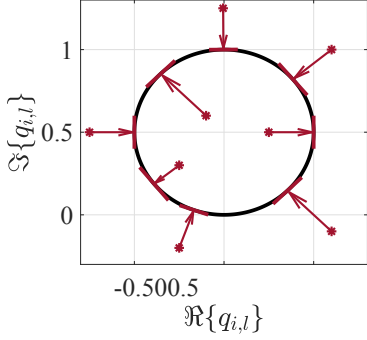


Fig. 2: Mapping the **P4** solution to the Lorentzian constrained weights in the complex plane.

$$\mathbf{P3} : \underset{\tilde{\mathbf{Q}}}{\text{minimize}} \quad \text{Tr}(\tilde{\mathbf{P}}_m^H \tilde{\mathbf{Q}}) \quad (20a)$$

$$\text{subject to} \quad \text{Tr}(\tilde{\mathbf{Z}}_{m,k}^H \tilde{\mathbf{Q}}) \geq \delta_k, \quad \forall k, \quad (20b)$$

$$\tilde{\mathbf{Q}} \succeq \mathbf{0}, \quad (20c)$$

$$q_{i,l} \in \mathcal{Q}, \quad \forall i, l, \quad (20d)$$

$$\text{rank}(\tilde{\mathbf{Q}}) = 1. \quad (20e)$$

Problem (20) is still difficult to solve due to the Lorentzian and rank constraints. Then, we relax the problem as

$$\mathbf{P4} : \underset{\tilde{\mathbf{Q}}}{\text{minimize}} \quad \text{Tr}(\tilde{\mathbf{P}}_m^H \tilde{\mathbf{Q}}) \quad (21a)$$

$$\text{subject to} \quad \text{Tr}(\tilde{\mathbf{Z}}_{m,k}^H \tilde{\mathbf{Q}}) \geq \delta_k, \quad \forall k, \quad (21b)$$

$$\tilde{\mathbf{Q}} \succeq \mathbf{0}. \quad (21c)$$

Hence, the problem becomes an SDP that can be solved similar to (16). Then, we transform the relaxed solution into a feasible solution according to constraints (20d) and (20e). First,  $\mathbf{q}'$  is obtained as the dominant eigenvector of  $\tilde{\mathbf{Q}}$  multiplied by the square root of its eigenvalue. Still,  $\mathbf{q}'$  is not Lorentzian constrained, thus, we map each of the elements in  $\mathbf{q}'$  to the nearest point on the Lorentzian constrained circle as represented in Fig. 2. Hereby, the configured phase of the  $l$ th metamaterial element in the  $i$ th microstrip can be obtained as

$$\phi_{i,l}^* = \min_{\phi_{i,l}} \left| \frac{j + e^{j\phi_{i,l}}}{2} - q'_{i,l} \right|, \quad \forall i, l, \quad (22)$$

where  $q'_{i,l}$  is the  $((i-1)N_h + l)$ th element in  $\mathbf{q}'$ , while (22) can be easily solved using a one-dimensional search. Then,

$$q_{i,l}^* = \frac{j + e^{j\phi_{i,l}^*}}{2}, \quad \forall i, l. \quad (23)$$

### C. Overall Algorithm

Algorithm 1 summarizes the overall EB optimization solution for DMA-assisted RF-WPT system. At first, a random Lorentzian constrained frequency response is generated for each metamaterial element, and  $\mathbf{Q}$  is constructed. Then, a local optimum solution is obtained for **P3** through lines 8-9, followed by finding the optimal precoders by solving **P2**. Moreover, the solution is updated in lines 12-15 if the transmit power decreases. The above process is repeated iteratively

### Algorithm 1 EB Optimization for DMA-based RF-WPT.

- 1: **Input:**  $c_{max}, I_{max}, \{\gamma_k, \delta_k\}_{\forall k}$
- 2: **Output:**  $\{\mathbf{w}_m^*\}_{\forall m}, \{q_{i,l}^*\}_{\forall i,l}$
- 3: **Initialize:**
- 4:  $iter = 1, c = 0$
- 5: Construct  $\mathbf{Q}$  using random  $\{\phi_{i,l}\}_{\forall i,l}$ , (9), and (10)
- 6: Solve **P2** to obtain  $P_{Tx}^*$  and  $\{\mathbf{w}_m^*\}_{\forall m}$
- 7: **repeat**
- 8: Solve **P4** to obtain  $\mathbf{q}'$
- 9: Obtain  $\{q_{i,l}\}_{\forall i,l}$  using (22) and (23) and construct  $\mathbf{Q}$
- 10: Solve **P2** to obtain  $P_{Tx}$  and  $\{\mathbf{w}_m\}_{\forall m}$
- 11:  $c \leftarrow c + 1$  and  $iter \leftarrow iter + 1$
- 12: **if**  $P_{Tx} < P_{Tx}^*$  **then**
- 13:  $P_{Tx}^* \leftarrow P_{Tx}, \mathbf{w}_m^* \leftarrow \mathbf{w}_m, q_{i,l}^* \leftarrow q_{i,l}, \forall m, i, l$
- 14:  $c \leftarrow 0$
- 15: **end if**
- 16: **until**  $c = c_{max}$  or  $iter = I_{max}$

until there is no improvement in the solution for a maximum stall counter or a maximum number of iterations is reached.

In the worst case, the algorithm solves two SDP problems for  $I_{max}$  iterations. Since SDP problems can be efficiently solved using interior point methods in polynomial time [16], the proposed algorithm converges in polynomial time.

## IV. NUMERICAL RESULTS

We consider a 100 m<sup>2</sup> indoor area with a transmitter at the center of the ceiling with a 3 m height. The users are randomly distributed over 30 realizations and  $\delta_k = 100 \mu\text{W}, \forall k$ , while the spacing between the DMA metamaterial elements and the microstrips are  $\lambda/5$  and  $\lambda/2$ , respectively. Thus,  $N_v = \lfloor \frac{L}{\lambda/2} \rfloor$  and  $N_h = \lfloor \frac{L}{\lambda/5} \rfloor$ . A @DuPont Piralux AP-9161 is utilized to design the microstrip line while its propagation coefficients are estimated for different frequencies as in Section II-A.

We refer to the proposed method as EB-ASD, while particle swarm optimization (PSO) [17] with 100 particles per iteration is used as a benchmark. The DMA performance is compared to the FD structure with an inter-element distance of  $\lambda/2$ . The optimal FD precoders are obtained by solving **P2** for  $P_{Tx} = \text{Tr}(\mathbf{W})$  and  $\mathbf{b}_k = \gamma_k$  as in [18]. Notably, an FD setup requires a considerably large number of RF chains with high power consumption, which is not considered here. Thus, the performance gap between DMA and FD may be even larger in practice. Notice that the channel and microstrip losses are calculated using (1) and (4), respectively.

Fig. 3 illustrates the simulation results over different operating frequencies. The proposed approach outperforms PSO, especially in the high-frequency regime. The reason is that the number of elements and problem space becomes significantly larger at higher  $f$ , and thus, PSO needs much more time and particles to perform well. Notice that although  $N$  increases with  $f$  in DMA and FD, the average  $P_{Tx}$  slightly changes. That is because the increased  $N$  compensates for the increased channel and microstrip losses. Notably, the number of utilizable elements in DMA is larger than in FD, and hence, it requires less transmit power to meet the EH requirements.

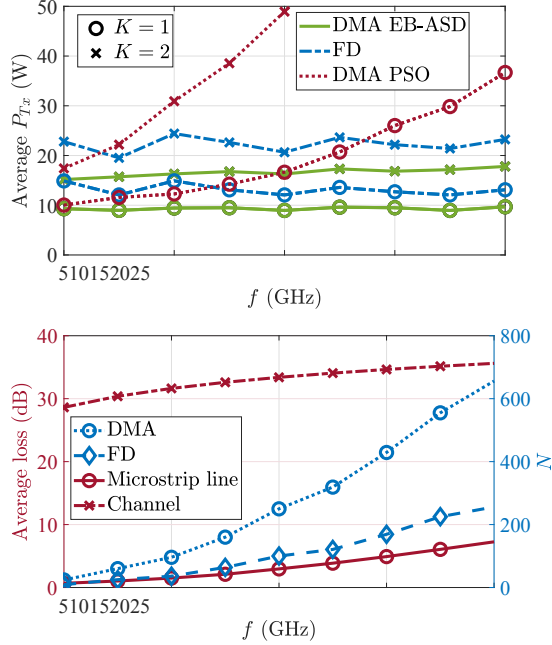


Fig. 3: (a) Average transmit power (top) and (b) average loss and the number of antenna elements (bottom), as a function of frequency for fixed  $L = 10$  cm,  $K = 1$ , and  $K = 2$ .

The influence of the antenna length is illustrated in Fig. 4. Notice that  $N$  increases with the antenna length while the average channel losses remain almost the same. The microstrip line loss slightly increases due to the additional propagation loss of the elements which are placed farther from the feeding point. Since the channel introduces significantly larger losses than the microstrip line, the average  $P_{Tx}$  reduces with  $L$  and more antenna elements can be utilized to meet the requirements and compensate for the loss. Furthermore, DMA outperforms FD, especially for smaller  $L$  and  $N$ . The proposed approach also outperforms PSO in this configuration.

## V. CONCLUSION

We considered a multi-user RF-WPT system with a DMA-based architecture. Moreover, we proposed an EB design aiming to minimize the transmit power while meeting the users' EH requirements. The solution, using SDP and alternating optimization, outperformed PSO. Our results also reveal that a DMA transmitter is preferred to the FD alternative, especially when the antenna array size is small. It was observed that although increasing the system frequency provides a larger number of elements, it does not affect the system performance due to the larger channel and microstrip losses. However, increasing the number of elements by utilizing a larger antenna array may promote significant performance gains because the channel and microstrip losses remain almost the same.

## REFERENCES

- [1] Z. Zhang *et al.*, "6G wireless networks: vision, requirements, architecture, and key technologies," *IEEE Veh. Technol. Mag.*, vol. 14, no. 3, pp. 28–41, 2019.
- [2] N. H. Mahmood *et al.*, "Six key features of machine type communication in 6G," in *2nd 6G SUMMIT*, pp. 1–5, 2020.

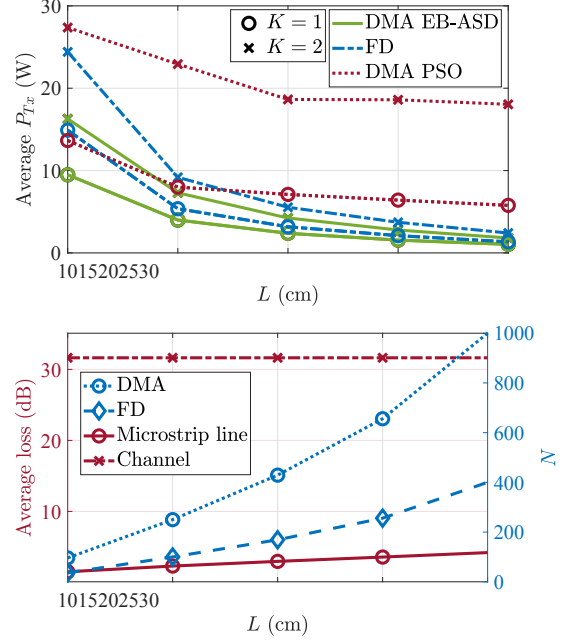


Fig. 4: (a) Average transmit power (top) and (b) average loss and the number of antenna elements (bottom), as a function of antenna length for fixed  $f = 10$  GHz,  $K = 1$ , and  $K = 2$ .

- [3] O. L. A. López *et al.*, "Massive wireless energy transfer: enabling sustainable IoT toward 6G era," *IEEE Internet Things J.*, vol. 8, no. 11, pp. 8816–8835, 2021.
- [4] B. Clerckx *et al.*, "Fundamentals of wireless information and power transfer: from RF energy harvester models to signal and system designs," *IEEE J. Sel. Areas Commun.*, vol. 37, no. 1, pp. 4–33, 2019.
- [5] I. Ahmed *et al.*, "A survey on hybrid beamforming techniques in 5G: architecture and system model perspectives," *IEEE Commun. Surv. Tutor.*, vol. 20, no. 4, pp. 3060–3097, 2018.
- [6] X. Gao *et al.*, "Energy-efficient hybrid analog and digital precoding for mmwave MIMO systems with large antenna arrays," *IEEE J. Sel. Areas Commun.*, vol. 34, no. 4, pp. 998–1009, 2016.
- [7] C. Lin and G. Y. Li, "Energy-efficient design of indoor mmwave and sub-THz systems with antenna arrays," *IEEE Trans. Wirel. Commun.*, vol. 15, no. 7, pp. 4660–4672, 2016.
- [8] L. Yan *et al.*, "A dynamic array-of-subarrays architecture and hybrid precoding algorithms for terahertz wireless communications," *IEEE J. Sel. Areas Commun.*, vol. 38, no. 9, pp. 2041–2056, 2020.
- [9] N. Shlezinger *et al.*, "Dynamic metasurface antennas for 6G extreme massive MIMO communications," *IEEE Wirel. Commun.*, vol. 28, no. 2, pp. 106–113, 2021.
- [10] H. Zhang *et al.*, "Near-field wireless power transfer with dynamic metasurface antennas," in *IEEE SPAWC*, pp. 1–5, 2022.
- [11] H. Zhang *et al.*, "Beam focusing for near-field multiuser MIMO communications," *IEEE Trans. Wirel. Commun.*, vol. 21, no. 9, pp. 7476–7490, 2022.
- [12] S. W. Ellingson, "Path loss in reconfigurable intelligent surface-enabled channels," in *IEEE PIMRC*, pp. 829–835, 2021.
- [13] D. R. Smith *et al.*, "Analysis of a waveguide-fed metasurface antenna," *Phys. Rev. Appl.*, vol. 8, p. 054048, Nov 2017.
- [14] D. M. Pozar, *Microwave engineering*. John Wiley & sons, 2011.
- [15] M. Grant and S. Boyd, "CVX: Matlab software for disciplined convex programming, version 2.1." <http://cvxr.com/cvx>, Mar. 2014.
- [16] R. Monteiro and T. Tsuchiya, "Polynomial convergence of primal-dual algorithms for the second-order cone program based on the MZ-family of directions," *Mathematical Programming, Series B*, vol. 88, pp. 61–83, 06 2000.
- [17] J. Kennedy and R. Eberhart, "Particle swarm optimization," in *Proc. Int. Conf. on Neural Networks*, vol. 4, pp. 1942–1948 vol.4, 1995.
- [18] O. L. A. López *et al.*, "Massive MIMO with radio stripes for indoor wireless energy transfer," *IEEE Trans. Wirel. Commun.*, vol. 21, no. 9, pp. 7088–7104, 2022.